

## Article

# Characterization of Products from the Aqueous-Phase Photochemical Oxidation of Benzene-Diols

Yang Ou <sup>1</sup>, Dongyang Nie <sup>2</sup>, Hui Chen <sup>1</sup>, Zhaolian Ye <sup>3</sup> and Xinlei Ge <sup>1,\*</sup>

<sup>1</sup> Jiangsu Key Laboratory of Atmospheric Environment Monitoring and Pollution Control (AEMPC), Collaborative Innovation Center of Atmospheric Environment and Equipment Technology (AEET), School of Environmental Science and Engineering, Nanjing University of Information Science & Technology (NUIST), Nanjing 210044, China; ouyang1085373017@163.com (Y.O.); 18252089278@163.com (H.C.)

<sup>2</sup> School of Atmospheric Sciences, Nanjing University, Nanjing 210023, China; dynie@nju.edu.cn

<sup>3</sup> College of Chemistry and Environmental Engineering, Jiangsu University of Technology, Changzhou 213001, China; bess\_ye@jsut.edu.cn

\* Correspondence: caxinra@163.com; Tel.: +86-25-5873-1394

**Abstract:** Chemical processing in atmospheric aqueous phases, including cloud and fog drops, might be significant in reconciling the gap between observed and modeled secondary organic aerosol (SOA) properties. In this work, we conducted a relatively comprehensive investigation of the reaction products generated from the aqueous-phase photochemical oxidation of three benzene-diols (resorcinol, hydroquinone, and methoxyhydroquinone) by hydroxyl radical ( $\cdot\text{OH}$ ), triplet excited state ( $^3\text{C}^*$ ) 3,4-dimethoxybenzaldehyde (3,4-DMB), and direct photolysis without any added oxidants. The results show that OH-initiated photo-degradation is the fastest of all the reaction systems. For the optical properties, the aqueous oxidation products generated under different reaction conditions all exhibited photo-enhancement upon illumination by simulated sunlight, and the light absorption was wavelength dependent on and increased as a function of the reaction time. The oxygen-to-carbon (O/C) ratio of the products also gradually increased against the irradiation time, indicating the persistent formation of highly oxygenated low-volatility products throughout the aging process. More importantly, aqueous-phase products from photochemical oxidation had an increased oxidative potential (OP) compared with its precursor, indicating they may more adversely impact health. The findings in this work highlight the importance of aqueous-phase photochemical oxidation, with implications for aqueous SOA formation and impacts on both the chemical properties and health effects of OA.



**Citation:** Ou, Y.; Nie, D.; Chen, H.; Ye, Z.; Ge, X. Characterization of Products from the Aqueous-Phase Photochemical Oxidation of Benzene-Diols. *Atmosphere* **2021**, *12*, 534. <https://doi.org/10.3390/atmos12050534>

Academic Editor: Jonathan Slade

Received: 15 March 2021

Accepted: 19 April 2021

Published: 22 April 2021

**Publisher's Note:** MDPI stays neutral with regard to jurisdictional claims in published maps and institutional affiliations.



**Copyright:** © 2021 by the authors. Licensee MDPI, Basel, Switzerland. This article is an open access article distributed under the terms and conditions of the Creative Commons Attribution (CC BY) license (<https://creativecommons.org/licenses/by/4.0/>).

**Keywords:** benzene-diols; oxidative potential; light absorption; secondary organic aerosol

## 1. Introduction

Secondary organic aerosol (SOA), an important component of fine particulate matter, plays an important role in haze formation, air quality, human health, and global climate change. For example, it may affect the aerosol optical properties and air quality because of the formation of light-absorbing organics and reactive oxygen species (ROS) [1–5]. SOA formation can take place in both gas and condensed phases. Much of the previous research on SOA has focused on the gas-phase reactions of volatile organic compounds [6,7]. In the last decade, an increasing number of studies have pointed out that chemical processing in atmospheric aqueous phases [8–10], such as cloud/fog drops and aqueous aerosols, is also an important pathway of SOA formation [8,11–16], which can also help fill the gap between observed and modeled particulate matter (PM) properties [17].

Phenols are important precursors of aqueous-phase SOA, and can be emitted significantly from biomass burning. Those phenols with high Henry's law constants can participate in hydroxyl radical (OH) and organic triplet excited state ( $^3\text{C}^*$ ) mediated aqueous phase

reactions, resulting in a high mass yield of SOA [18–23]. Resorcinol, hydroquinone, and methoxyhydroquinone are three representative organic compounds with near source concentrations up to ~50 ppbv in biomass burning plumes [24]. These benzene-diols, together with polyfunctional groups, are ubiquitous in the atmosphere as testified by the qualitative analysis of cloud water samples that were impacted by biomass burning [25,26], suggesting the great possibilities of these aromatic species undertaking oxidizing reactions in aqueous phase. A few studies have explored the chemical mechanisms of oxidation of several dihydroxybenzenes at the air–water interface by O<sub>3</sub> and hydroxyl radicals [27–30]. However, knowledge about the physical and chemical properties, as well as the biological toxicity of the aqueous oxidation products from those species, is still limited.

In this work, we investigated the photochemical aqueous-phase oxidation of three benzene-diols (resorcinol, hydroquinone, and methoxyhydroquinone) by hydroxyl radical (OH), triplet excited state (<sup>3</sup>C\*) from 3,4-dimethoxybenzaldehyde (3,4-DMB), and by direct photolysis without any added oxidants in bulk solutions. For each combination of precursors with/without oxidants, we measured the decay rates, optical properties, bulk chemical composition, and oxidative potential of the aqueous-phase products, in order to provide useful insight into understanding the formation mechanism and impacts of aqueous-phase processing on biomass burning emissions.

## 2. Materials and Methods

### 2.1. Aqueous-Phase Oxidation Experiments

The aqueous-phase photochemical oxidation reactions of resorcinol (RES), hydroquinone (HQ), and methoxyhydroquinone (MHQ) were conducted under three conditions, namely: (A) hydroxyl radical (OH) from hydrogen peroxide, (B) triplet excited states of organic compounds (<sup>3</sup>C\*) generated from 3,4-dimethoxybenzaldehyde (3,4-DMB), and (C) direct photolysis without any added oxidants. The oxidation was performed inside a photoreactor (BILON-GHX-ID, BiLang Company, Shanghai, China) equipped with a 1000 W Xe lamp, which was used to simulate natural sunlit conditions. A magnetic stirrer and a recirculating chiller were used to keep the reaction system at a constant temperature of 25 °C. Six quartz cuvettes (length \* outer diameter \* inner diameter (mm) = 190 \* 36 \* 34), each containing 100 mL of solution, were arranged equidistantly around the lamp in the photoreactor.

We chose an initial concentration of 100 μM for the benzene-diols, 5 μM for 3,4-DMB, and 100 μM for H<sub>2</sub>O<sub>2</sub>, considering the actual atmospheric levels of these species [31–37] and those used in other similar experiments [12,19,38,39]. It should be noted that in this work, 10 mg/L (NH<sub>4</sub>)<sub>2</sub>SO<sub>4</sub> was added in the aqueous solutions to mimic the ambient aerosol composition and to act as an internal standard to quantify the organic mass measured by the soot particle aerosol mass spectrometry (SP-AMS) [40,41] (details in Section 2.4). The solution was also simultaneously adjusted to a pH of 5 by using sulfuric acid using sulfuric acid. We also conducted dark control experiments under the same conditions by turning off the Xe lamp and covering the solution vials with aluminum foil. The experimental conditions and the analyses conducted are summarized in Table S1 in the Supplementary Materials.

### 2.2. Decay Kinetics of Benzene-Diols

Each series of oxidation experiments was carried out until approximately half of the precursors were degraded, during which the concentrations of the remaining precursor was measured periodically by a high-performance liquid chromatograph (HPLC; Waters, C18-WP column, 4.6 × 250 mm, 5 μm) with a UV–visible spectrometer in sampled solutions. A mobile phase of 70% acetonitrile and 30% water at a flow rate of 0.7 mL/min was used for the isocratic elution.

The apparent first-order rate constant ( $k_d$ ) of loss of precursor was then determined by the following equation:

$$\ln\left(\frac{[\text{ArOH}]_t}{[\text{ArOH}]_0}\right) = -k_d t \quad (1)$$

where  $[\text{ArOH}]_t$  and  $[\text{ArOH}]_0$  refer to the measured concentrations of precursors at times  $t$  and 0, respectively.

### 2.3. Light Absorptive Properties of Products

We examined the light absorption spectra of the aqueous-phase reaction products at different reaction times by using UV-VIS spectroscopy (UV-3600, Shimadzu, Tokyo, Japan). Combined with the total organic carbon (TOC) content from the TOC analyzer (Shimadzu, Tokyo, Japan), the wavelength dependent mass absorption coefficient (MAC) of the products can be calculated based on Equation (2):

$$\text{MAC} = \frac{A \times \ln 10}{b \times C_{\text{mass}}} \quad (2)$$

where  $A$  is the light absorbance measured at a certain wavelength,  $b$  is the light path length of the liquid sample capillary waveguide, and  $C_{\text{mass}}$  is the TOC mass concentration.

### 2.4. Chemical Analyses of Products by the SP-AMS

Here, the SP-AMS employed the 70 eV electron impact ionization technique coupled with a time-of-flight mass spectrometer (ToF-MS), and was used to determine the mass spectrum of aqueous-phase products. The mass spectrum was a collection of 70 eV EI ionized fragments, which represented the bulk chemical properties of all of the products. The technical details of the SP-AMS have been described previously [18,42,43]. In this work, we used the SP-AMS, but turned off the laser vaporizer, so the SP-AMS was the same as the HR-AMS. The similar SP-AMS measurements were conducted by our group previously for the characterization of aqueous-phase photochemical oxidation products [20,21]. Briefly, during the SP-AMS measurement, a continuous flow of the reacted solution was drawn using a miniature pump at a rate of 1 mL/min, and the solution was nebulized by pressurized argon gas to generate particles, which then passed through the diffusion drier filled with silicon in order to remove the moisture before entering into the SP-AMS [44]. It is of note that during this process, some products with high volatility might partition into the gas phase; however, this process in fact mimics the water evaporation of fog/cloud droplets in the real atmosphere. The SP-AMS analyses were conducted on OH- and  $^3\text{C}^*$ -initiated photo-oxidation experiments.

The SP-AMS data were analyzed using the Igor-based ToF-AMS Analysis Toolkit (Squirrel v.1.57 A and Pika v1.16 A [45]). The time resolution was 1.5 min and ion fragments with a mass-to-charge ( $m/z$ ) ratio up to 300 were recorded. The directly measured organic  $\text{CO}_2^+$  and  $\text{H}_2\text{O}^+$  signals were used here by assuming no significant influences from air or water (because we used Argon as protective gas and the particles were dried before measurement). As for  $\text{HO}^+$  and  $\text{O}^+$  signals, we scaled them by  $\text{HO}^+ = 0.5625 \times \text{CO}_2^+$  and  $\text{O}^+ = 0.009 \times \text{CO}_2^+$  [46]. The atomic elemental ratios, including the oxygen-to-carbon (O/C) ratio, hydrogen-to-carbon (H/C) ratio, and the carbon oxidation state (OSc; equal to  $2 \times \text{O/C} - \text{H/C}$ ) of the products were calculated according to "Improved-Ambient" method reported previously [47]. More details can be found in our previous studies [41,48].

### 2.5. Positive Matrix Factorization (PMF) of the Aqueous-Phase Products

PMF is typically used to resolve a limited number of factors that can reconstruct the observed time series of organics, and each factor is a collection of species with similar properties and atmospheric behaviors [49,50]. In this study, the PMF algorithm was employed to explore the different generations of aqueous-phase oxidation products and their chemical properties. All ions with  $m/z$  up to 300 were used for the PMF analyses. However, for ions with  $m/z > 150$ , only those with significantly large signal-to-noise (S/N) ratios were

fitted because of the limited chemical resolution. In addition, the directly measured organic data matrices, as well as the corresponding error matrices, were normalized by the sulfate (internal standard) concentrations. The organic matrices were also pretreated following our previous studies [10,39], including downweight of “weak” values ( $0.2 < S/N < 2$ ), removal of “bad” values ( $S/N < 0.2$ ), and downweight of outliers (specific  $m/z$ s or time points that have large influences on  $Q/Q_{\text{exp}}$ ). We explored the PMF solutions by varying the  $f_{\text{peak}}$  values from -1 to 1 with a step of 0.1 for 1 to 4 factors. No significant differences were found for the same solution at different  $f_{\text{peak}}$  values, we therefore chose the one at an  $f_{\text{peak}}$  of 0. Note that the four-factor solution had no appreciable improvements on the fitting results and the mass spectra of two of the four factors were similar. A three-factor solution was therefore chosen to be the best one. The three-factor solution was actually common for chamber or aqueous-phase derived SOA in a few previous studies [10,51].

### 2.6. Oxidative Potential (OP) of Products Based on Dithiothreitol (DTT) Assay

The DTT assay measures the reactive oxygen species (ROS) via the formation of DTT disulfide as a result of transferred electrons from DTT to oxygen [52], and the DTT consumption rate can be used to represent the OP. In this work, for each precursor, the OPs of the starting solution with a pure precursor (but no oxidant), and those oxidized solutions at about a half lifetime, were quantified by DTT analysis. All of the samples were stored at  $-20\text{ }^{\circ}\text{C}$  in Teflon tubes under dark conditions, and the OP measurements were conducted for no longer than a week after sampling in order to ensure the effectiveness of results. First, 3.5 mL of the sample was incubated with 1 mL phosphate buffer (PBS) and 0.5 mL (1 mM) DTT solution in a water bath incubator ( $37\text{ }^{\circ}\text{C}$ ). During each OP analysis, a small aliquot of the DTT and sample mixture was withdrawn at fixed time intervals (5, 10, 20, 30, 45, and 60 min), and was then mixed with trichloroacetic acid (TCA; 1%  $w = v$ ) to quench the DTT reactions. Then, 0.5 mL of 5,5'-dithiobis-(2-nitrobenzoic acid) (DTNB) and 1 mL of Tris buffer (pH  $\sim 8.9$ ) were added, and the remaining DTT was reacted with DTNB to form a colored product that absorbed light at 412 nm. The light absorption of the mixture at 412 nm was measured using a spectrophotometer (SpectraMax iD3, Molecular Devices, San Jose, CA, USA). The rate of DTT consumption was determined using the linear regression of a series of absorbance data versus time. Based on the average of six duplicate measurements, a value expressed as nmol DTT/min per mL can represent the OP of the corresponding sample.

## 3. Results and Discussion

### 3.1. Kinetic Study

The apparent first-order rate constants can be used to represent the degradation rates of the benzene-diols, but they are dependent on the light flux, intersystem crossing efficiency, diluted oxygen concentration, etc. Note that in this study, we mainly focused on the analyses of aqueous-phase oxidation products, and this section only compares the degradation rates due to the influences of different oxidants among benzene-diols under the same experiment conditions (same precursor and oxidant concentration and the same light flux), so the influences of other factors (light flux and intersystem crossing efficiency) on the rate constants were not further discussed. To be close to the actual atmosphere, our reaction conditions were under simulated natural sunlit conditions (1000 W Xe lamp), and contained inorganic salts. In the future, explicit kinetic studies that measure second-order rate constants [20,21,38] can be conducted in order to make the kinetic parameters applicable over other conditions.

Figure 1 shows the degradations of RES, HQ, and MHQ under illumination and dark conditions. It can be found that direct photolysis could occur for all three phenolic compounds. The rate constants of direct photo-degradation were 0.022, 0.035, and  $0.23\text{ h}^{-1}$  for RES, HQ, and MHQ, respectively. The largest rate constant was for MHQ, likely because methoxy can act as an electron donor, which greatly enhances the charge density of the benzene ring. It is noted that the addition of 3,4-DMB did not significantly accelerate their

direct photolysis rates, likely because the formation of  $^3\text{C}^*$  of phenols themselves was more efficient than the  $^3\text{C}^*$  of 3,4-DMB. OH-initiated photo-degradation was faster than the direct photolysis and the photolysis against  $^3\text{C}^*$  for RES and HQ, but the effect was not obvious for MHQ, mainly because the degradation of MHQ was much quicker than for RES and HQ. The rate constants for the decay of benzene-diols under different conditions varied from  $0.022\text{ h}^{-1}$  to  $0.26\text{ h}^{-1}$ , together with  $t_{1/2}$  (half-lifetime) from 154 min to 1697 min (Table S2), generally on the same order of decay rates of benzene-diols determined in other works [41,48,53,54].

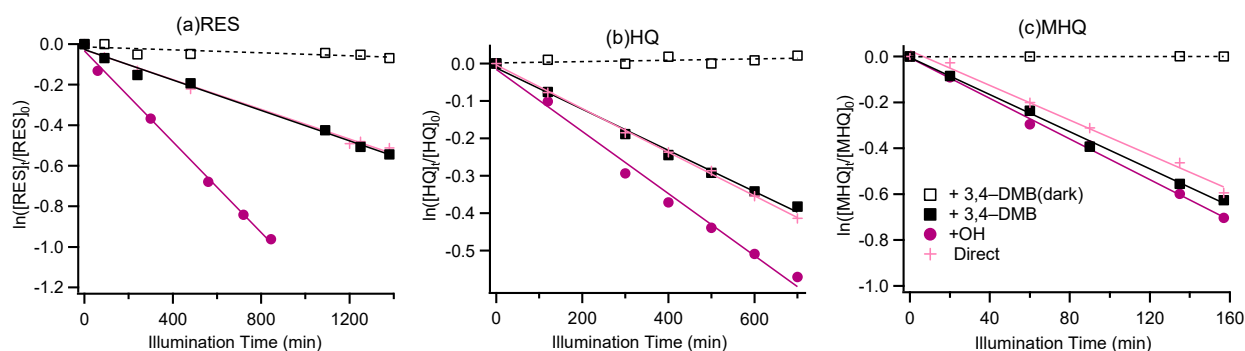


**Figure 1.** Aqueous-phase decay kinetic curves for (a) resorcinol (RES), (b) hydroquinone (HQ), and (c) methoxyhydroquinone (MHQ).

### 3.2. Light Absorption Properties

Atmospheric brown carbon (BrC) is a collective term for light absorbing organic compounds in the atmosphere; it drew our attention for its importance in scattering and absorbing solar radiation [53,54]. In addition to primary sources (i.e., biomass burning), BrC can also be produced from secondary reaction process including gas-phase and aqueous-phase reactions [55,56]. In this work, we also investigated whether or not the aqueous-phase reactions of the selected precursors could produce light-absorbing species. From the UV–VIS light absorption spectra presented in Figure S1, we can clearly observe that the aqueous-phase photochemical reactions under all conditions increased the light absorption ability over its precursor, and the enhancement of light absorption increased with the increase of the reaction time. In particular, an obvious absorption at 450–500 nm could be found in HQ oxidation systems. Overall, the light absorption was wavelength dependent, which was high in the ultraviolet range and then decreased with the increase in wavelength for all of the reaction systems.

Figure 2 presents the light absorption enhancement (the ratio of light absorption at a certain time relative to that of the initial solution) during oxidation in the UV and visible light ranges, respectively. For RES, the products from the  $^3\text{C}^*$ -mediated photochemical oxidation appeared to generate more visible light absorbing species, while OH-mediated oxidation produced UV light absorbing species; for HQ, more visible light absorbing organics were generated too, but the species from direct photolysis instead had the strongest visible light absorbing ability; for MHQ,  $^3\text{C}^*$ -oxidation products had a strong light absorption in both UV and visible light ranges. Furthermore, 400 nm was chosen as a representative wavelength to demonstrate the light absorbing abilities of the oxidation products. The MAC values at all wavelengths of all systems at their oxidation endpoints, as well as the MAC values at 400 nm versus the O/C ratios for the OH- and  $^3\text{C}^*$ -oxidation experiments, are shown in Figure 3. The MAC value of the aqueous-phase products decreased against the wavelength and increased against the O/C values. This was in part due to the production of carboxylic and carbonyl compounds from the aqueous reactions. It should also be noted that the MAC values of our aqueous-phase oxidation products were  $10 \times$  as high as those SOA from the gas-phase oxidation of the biomass burning emissions [57], which highlights the potentially large impact of aqueous-phase processing on the radiative forcing of aerosols in the real atmosphere.

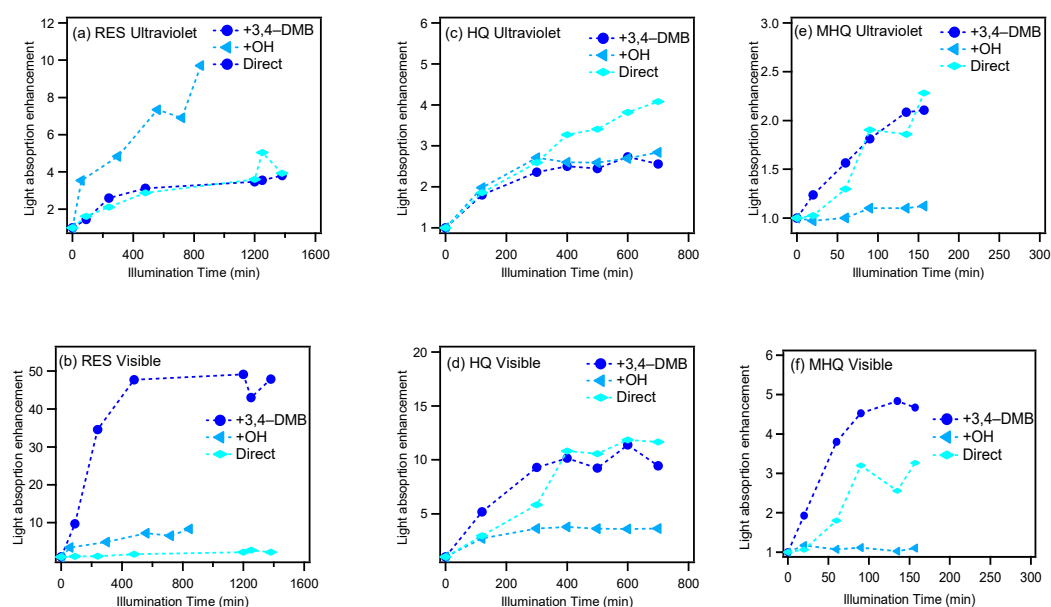


**Figure 2.** Variations of the light absorption enhancement (ratio of light absorption at the sampling time to that at the starting point) with illumination time in ultraviolet (200–380 nm) and visible light (380–600 nm) ranges, respectively.

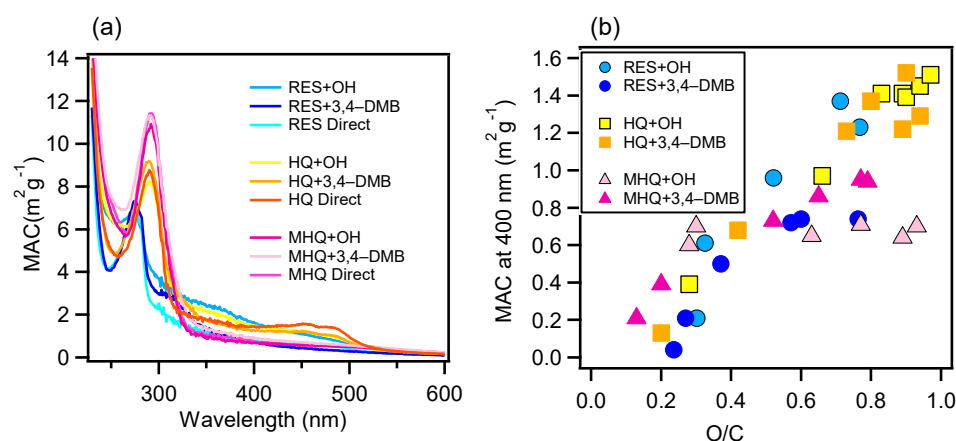


**Figure 3.** (a) Mass absorption coefficient (MAC) values as a function of the wavelength of the final solutions and (b) MAC values at 400 nm versus the oxygen-to-carbon (O/C) ratios of the solutions during different times of the OH- and  $^3\text{C}^*$ -mediated oxidation experiments.

### 3.3. Chemical Properties and Evolution of Aqueous Oxidation Products

SP-AMS-measured high resolution mass spectra of the aqueous-phase oxidation products from all six systems presented ion fragments with relatively high  $m/z$  values during the initial stage of photochemical oxidation. For example, Figure 4 shows the mass spectra of oxidation products during different reaction times in MHQ + OH and MHQ + 3,4-DMB systems, respectively. It can be seen that the relative abundance of large  $m/z$  ions gradually decreased with the increase in reaction time, while the fractional contributions of  $\text{CO}_2^+$  ( $m/z = 44$ ),  $\text{H}_2\text{O}^+$  ( $m/z = 18$ ), and  $\text{CO}^+$  ( $m/z = 28$ ) increased; the mass spectra became similar to the pattern of the fulvic acid, which could represent highly oxidized organics [58], and indeed the O/C ratio increased greatly with the propagation of oxidation. The mass spectra of oxidation products from other benzene-diols showed similar chemical features (Figures S2 and S3), indicating a generally similar oxidation mechanism, likely including hydroxylation, oligomerization, functionalization, and fragmentation [19].

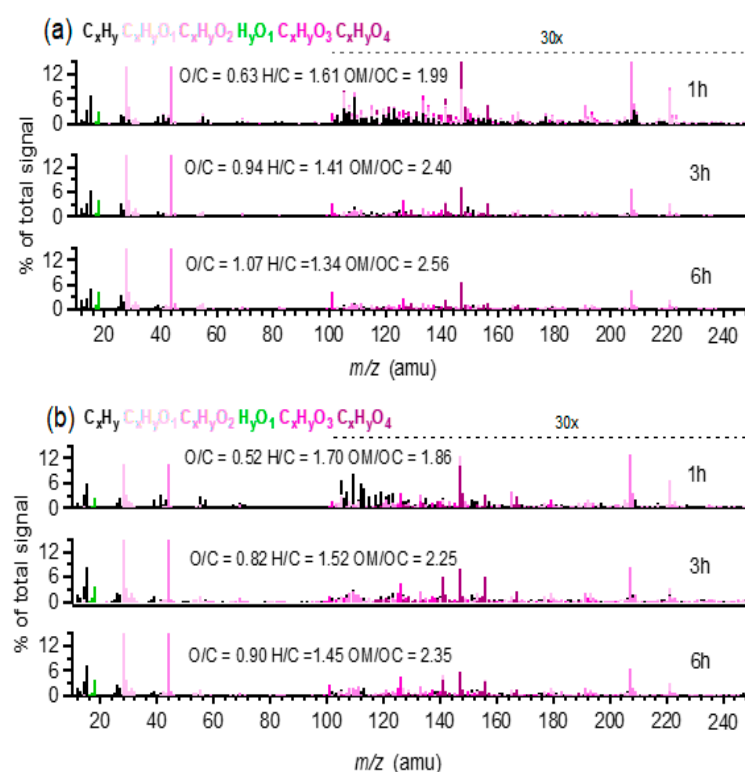


**Figure 4.** High resolution mass spectra of (a) MHQ + OH and (b) MHQ+3,4-DMB at different reaction times. The hydrogen-to-carbon (H/C) and O/C ratios and  $OS_c$  values are also shown for each mass spectrum. The colored sticks represent the following six ion families:  $C_xH_y$ ,  $C_xH_yO_1$ ,  $C_xH_yO_2$ ,  $H_yO_1$ ,  $C_xH_yO_3$ , and  $C_xH_yO_4$ . The ion signals at  $m/z > 100$  are amplified  $30 \times$  for clarity.

The variations of the elemental ratios of the aqueous-phase products are shown in Figure 5. As we can see, the O/C and  $OS_c$  increased, while H/C decreased continuously throughout the reaction, suggesting that highly oxidized products were produced consistently during aqueous oxidation of all three precursors. We also used the  $f_{44}$  (mass ratio of  $m/z$  44 to the total organics) versus  $f_{43}$  (mass ratio of  $m/z$  43 to the total organics) plot to investigate the evolution of aqueous oxidation products (Figure S4a). In this plot, the data points moved towards the upper left corner with the increase of oxidation. In addition, we also used van Krevelen diagram (O/C versus H/C) to further investigate the possible oxidation pathways. As shown in Figure S4b, the slopes were close to  $-1$ , likely indicating oxidation similar to the pathway of the formation of carboxylic acids. The O/C value of the aqueous-phase products from each experiment approached end values of 0.8–1.1, which were at the same level of previously reported aqueous-phase SOA [8,59]. The  $OS_c$  of aqueous-phase products at the termination of reactions were much higher than their precursors, further demonstrating that the aqueous-phase photooxidation is an important source of oxygenated species in the atmosphere.

Furthermore, the PMF analysis was used to explore the chemical evolution of aqueous-phase products. The temporal variations of the three-factor PMF solution for each experiment are presented in Figure 6, and the diagnostic plots of the representative MHQ + OH experiment are shown in Figure S5. For six series of experiments, the PMF analyses all resolved a factor with the lowest O/C (i.e., factor 1), which might be initial (first-generation) products; as the mass concentration of this factor continuously decreased and became very small at the end of the experiment, indicating its fragmentation upon further oxidation. Factor 2, with a medium O/C level, might represent intermediated products (second-generation), as its concentration increased first then decreased afterwards; it may involve the transformation from Factor 1 first, then fragmentation later on. Factor 3 had the highest O/C, and its concentration persistently increased; it may involve chemical transformation

from Factor 1 in the first stage, and then significantly from Factor 2 in later stages, as it increased while Factor 2 decreased quickly. This factor represented the final oxidation products (third-generation), as in the end, Factor 1 and Factor 2 almost disappeared. The variations of PMF factors, as well as the changes of mass spectral features (Figure 4), indicate that the oxidation pathway was first dominated by hydroxylation/oligomerization, then functionalization and fragmentation in the end.

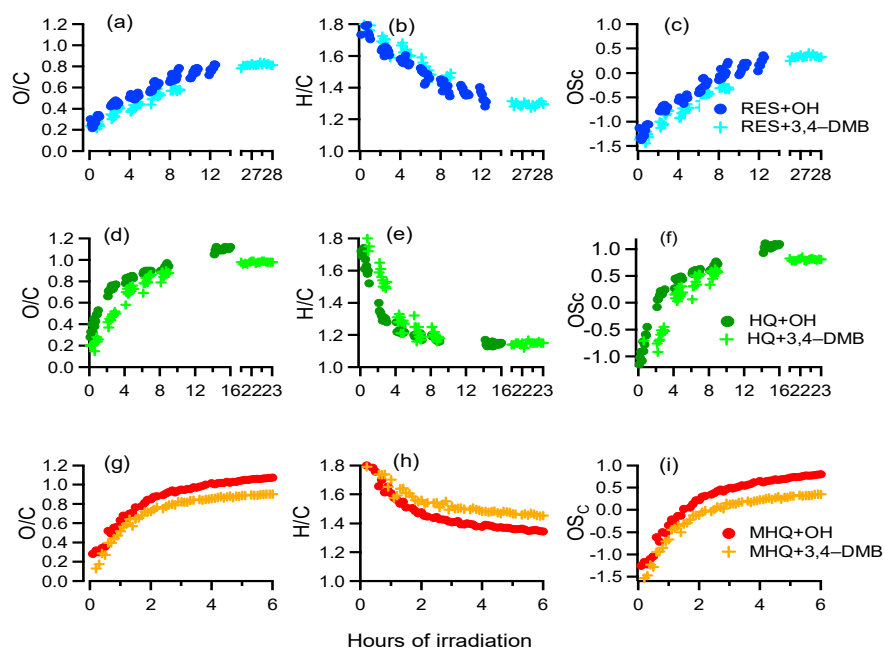


**Figure 5.** (a,d,g) O/C of aqueous-phase products, (b,e,h) H/C of aqueous-phase products, and (c,f,i) OS<sub>c</sub> of aqueous-phase products as a function of time during different experiments.

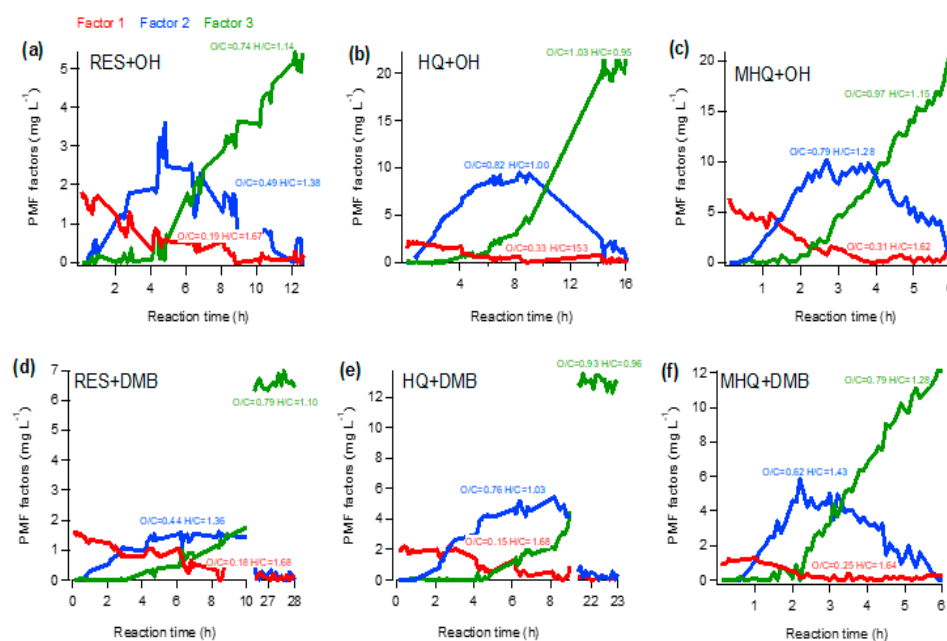


**Figure 6.** Temporal variations of the three factors from the positive matrix factorization (PMF) analyses of aqueous-phase products in the oxidation of (a,d) MHQ, (b,e) RES, and (c,f) HQ. The O/C and H/C of each factor are also shown.

### 3.4. Oxidative Potential of Aqueous-Phase Products Compared with the Precursor

The presence of reactive oxygen species (ROS) or free radicals can induce oxidative stress (known as oxidative potential (OP)), which is considered to be an important mechanism for particle-associated adverse health effects [60–62]. Although previous work has reported on the toxicity of photochemically aged SOA in the gas phase [63], little is known about the toxicity from the SOA formed in the aqueous-phase pathway. The OPs of the initial precursor solution and their aqueous-phase oxidation products are shown in Figure 7.

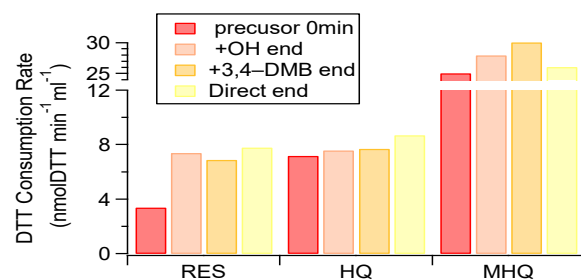


**Figure 7.** Dithiothreitol (DTT) consumption rates of aqueous-phase oxidation products and the corresponding pure precursors. The 0 min samples represent solutions containing only 100  $\mu\text{M}$  precursor with no oxidants, while the end samples were taken at the end of the experiments (about half precursor was consumed).

For the pure precursors, the OP of MHQ was the highest, followed by HQ and RES.

The products formed from the photochemical aqueous oxidation appeared to consistently enhance its OP (especially for RES) under different experiment conditions (i.e., various kinds of oxidants). These results underscore that aqueous-phase processing led to the production of more toxic species [64], and further investigations are therefore needed on a broad spectrum of species and indicators of toxicity in order to better understand the role of aqueous-phase processing on particle toxicity.

## 4. Conclusions

In this work, we investigated the aqueous-phase photochemical oxidation of three benzene-diols (resorcinol, hydroquinone, and methoxyhydroquinone). We found that direct photolysis could occur in all three species. The addition of an OH oxidant could further promote oxidation, while the addition of  $^3\text{C}^*$  of 3,4-DMB had only small influences on the photolysis rates. The optical measurements of the oxidation products showed that aqueous-phase processing could produce strong light absorbing species, and the MAC values of the products decreased against the wavelength and increased with the oxidation degree of the products. The light absorption enhancement from  $^3\text{C}^*$ -mediated oxidation was more significant, especially in the visible light range. The oxygen-to-carbon (O/C) and  $\text{OS}_c$  values of the aqueous-phase products at the end of the reactions were much higher than their corresponding precursors, demonstrating that the aqueous-phase photooxidation of organic precursors could be an important source of oxygenated species in the atmosphere. In addition, aqueous-phase processing also enhanced the OP of precursor in all of the tested conditions, highlighting that aqueous-phase processing led to the formation of more toxic species. Our results underscore the aqueous-phase photooxidation on the modification of the chemical, optical as well as toxic properties of atmospheric organics, and also call for more studies on other types of precursors.

**Supplementary Materials:** The following are available online at <https://www.mdpi.com/article/10.3390/atmos12050534/s1>, Table S1: Summary of experimental conditions and relevant analyses, Table S2. Summary of the kinetic parameters of the benzene-diols precursors, Figure S1: Time-dependent UV-Vis light absorption spectra of the reacted solutions obtained at different times during the oxidation experiments, Figure S2: Mass spectra of (a) RES+OH and (b) RES+3,4-DMB at different

reaction times. The H/C, O/C ratios and OSc values are also shown. The colored sticks represent 6 ion families:  $C_xH_y$ ,  $C_xH_yO_1$ ,  $C_xH_yO_2$ ,  $H_yO_1$ ,  $C_xH_yO_3$  and  $C_xH_yO_4$ . The ion signals at  $m/z > 100$  are amplified 30 times for clarity, Figure S3. Mass spectra of (a) HQ + OH and (b) HQ+3,4-DMB at different reaction times. The H/C, O/C ratios and OSc values are also shown. The colored sticks represent 6 ion families:  $C_xH_y$ ,  $C_xH_yO_1$ ,  $C_xH_yO_2$ ,  $H_yO_1$ ,  $C_xH_yO_3$  and  $C_xH_yO_4$ . The ion signals at  $m/z > 100$  are amplified 30 times for clarity, Figure S4. Evolution profiles of aqueous-phase SOA: (a)  $f_{44}$  (mass ratio of ion signal at  $m/z$  44 to total organic signal) vs.  $f_{43}$  (mass ratio of ion signal at  $m/z$  43 to total organic signal). (b) Van Krevelen (VK) diagram based on AMS data, in which lines with slopes of 0,  $-1$  and  $-2$  represent the reaction pathways with additions of alcohol/peroxide, carboxylic acid, and ketone/aldehyde functional group, respectively. Dashed lines are OSc values, Figure S5. Three-factor solution for PMF analysis of OH-mediated oxidations of MHQ.

**Author Contributions:** Conceptualization, X.G.; data curation, Y.O., D.N., and Z.Y.; formal analysis, Y.O., D.N., and H.C.; funding acquisition, X.G.; investigation, H.C.; methodology, Y.O., H.C., Z.Y., and X.G.; supervision, Z.Y. and X.G.; writing—original draft, Y.O., D.N., and X.G. All authors have read and agreed to the published version of the manuscript.

**Funding:** This research was funded by the Natural Science Foundation of China (21976093, 91544220, and 42021004) and the China Post-Doctoral Science Foundation (no. 2019M661790).

**Institutional Review Board Statement:** Not applicable.

**Informed Consent Statement:** Not applicable.

**Data Availability Statement:** The data used in this study can be made available upon request ([caxinra@163.com](mailto:caxinra@163.com)).

**Acknowledgments:** We acknowledge the Support from other group members (Shijie Cui, Yanfang Chen) for the technical support.

**Conflicts of Interest:** The authors declare no conflict of interest.

## References

1. Zhang, Q.; Jimenez, J.L.; Canagaratna, M.R.; Allan, J.D.; Coe, H.; Ulbrich, I.; Alfarra, M.R.; Takami, A.; Middlebrook, A.M.; Sun, Y.L.; et al. Ubiquity and dominance of oxygenated species in organic aerosols in anthropogenically-influenced Northern Hemisphere midlatitudes. *Geophys. Res. Lett.* **2007**, *34*, 29979–29986. [[CrossRef](#)]
2. Hu, J.; Ying, Q.; Wang, Y.; Zhang, H. Characterizing multi-pollutant air pollution in China: Comparison of three air quality indices. *Environ. Int.* **2015**, *84*, 17–25. [[CrossRef](#)] [[PubMed](#)]
3. Nie, D.; Chen, M.; Wu, Y.; Ge, X.; Hu, J.; Zhang, K.; Ge, P. Characterization of Fine Particulate Matter and Associated Health Burden in Nanjing. *Int. J. Environ. Res. Public Health* **2018**, *15*, 602. [[CrossRef](#)]
4. Nie, D.; Wu, Y.; Chen, M.; Liu, H.; Zhang, K.; Ge, P.; Yuan, Y.; Ge, X. Bioaccessibility and health risk of trace elements in fine particulate matter in different simulated body fluids. *Atmos. Environ.* **2018**, *186*, 1–8. [[CrossRef](#)]
5. Mayorga, R.J.; Zhao, Z.; Zhang, H. Formation of secondary organic aerosol from nitrate radical oxidation of phenolic VOCs: Implications for nitration mechanisms and brown carbon formation. *Atmos. Environ.* **2021**, *244*, 117910. [[CrossRef](#)]
6. Wang, H.; Gao, Y.; Wang, S.; Wu, X.; Liu, Y.; Li, X.; Huang, D.; Lou, S.; Wu, Z.; Guo, S.; et al. Atmospheric Processing of Nitrophenols and Nitrocresols From Biomass Burning Emissions. *J. Geophys. Res. Atmos.* **2020**, *125*, 33401–33413. [[CrossRef](#)]
7. Akherati, A.; He, Y.; Coggon, M.M.; Koss, A.R.; Hodshire, A.L.; Sekimoto, K.; Warneke, C.; A De Gouw, J.; Yee, L.D.; Seinfeld, J.H.; et al. Oxygenated Aromatic Compounds are Important Precursors of Secondary Organic Aerosol in Biomass-Burning Emissions. *Environ. Sci. Technol.* **2020**, *54*, 8568–8579. [[CrossRef](#)]
8. Gilardoni, S.; Massoli, P.; Paglione, M.; Giulianelli, L.; Carbone, C.; Rinaldi, M.; Decesari, S.; Sandrini, S.; Costabile, F.; Gobbi, G.P.; et al. Direct Observation of Aqueous Secondary Organic Aerosol from Biomass-Burning Emissions. *Proc. Natl. Acad. Sci. USA* **2016**, *113*, 10013–10018. [[CrossRef](#)] [[PubMed](#)]
9. Wang, J.; Wang, G.; Wu, C.; Li, J.; Cao, C.; Li, J.; Xie, Y.; Ge, S.; Chen, J.; Zeng, L.; et al. Enhanced aqueous-phase formation of secondary organic aerosols due to the regional biomass burning over North China Plain. *Environ. Pollut.* **2020**, *256*, 113401. [[CrossRef](#)]
10. Lu, J.; Ge, X.; Liu, Y.; Chen, Y.; Xie, X.; Ou, Y.; Ye, Z.; Chen, M. Significant secondary organic aerosol production from aqueous-phase processing of two intermediate volatility organic compounds. *Atmos. Environ.* **2019**, *211*, 63–68. [[CrossRef](#)]
11. Engelhart, G.J.; Hennigan, C.J.; Miracolo, M.A.; Robinson, A.L.; Pandis, S.N. Cloud condensation nuclei activity of fresh primary and aged biomass burning aerosol. *Atmos. Chem. Phys. Discuss.* **2012**, *12*, 7285–7293. [[CrossRef](#)]
12. Ding, Z.; Du, W.; Wu, C.; Cheng, C.; Meng, J.; Li, D.; Ho, K.; Zhang, L.; Wang, G. Summertime atmospheric dicarboxylic acids and related SOA in the background region of Yangtze River Delta, China: Implications for heterogeneous reaction of oxalic acid with sea salts. *Sci. Total Environ.* **2021**, *757*, 143741. [[CrossRef](#)]

13. Duan, J.; Huang, R.-J.; Gu, Y.; Lin, C.; Zhong, H.; Wang, Y.; Yuan, W.; Ni, H.; Yang, L.; Chen, Y.; et al. The formation and evolution of secondary organic aerosol during summer in Xi'an: Aqueous phase processing in fog-rain days. *Sci. Total Environ.* **2021**, *756*, 144077. [[CrossRef](#)] [[PubMed](#)]
14. Ervens, B.; Turpin, B.J.; Weber, R.J. Secondary organic aerosol formation in cloud droplets and aqueous particles (aqSOA): A review of laboratory, field and model studies. *Atmos. Chem. Physics.* **2011**, *11*, 11069–11102. [[CrossRef](#)]
15. Wang, J.; Ye, J.; Zhang, Q.; Zhao, J.; Wu, Y.; Li, J.; Liu, D.; Li, W.; Zhang, Y.; Wu, C.; et al. Aqueous production of secondary organic aerosol from fossil-fuel emissions in winter Beijing haze. *Proc. Natl. Acad. Sci. USA* **2021**, *118*, 118. [[CrossRef](#)]
16. Ge, X.; Zhang, Q.; Sun, Y.; Ruehl, C.R.; Setyan, A. Effect of aqueous-phase processing on aerosol chemistry and size distributions in Fresno, California, during wintertime. *Environ. Chem.* **2012**, *9*, 221–235. [[CrossRef](#)]
17. Ervens, B. Modeling the Processing of Aerosol and Trace Gases in Clouds and Fogs. *Chem. Rev.* **2015**, *115*, 4157–4198. [[CrossRef](#)]
18. Sun, Y.L.; Zhang, Q.; Anastasio, C.; Sun, J. Insights into secondary organic aerosol formed via aqueous-phase reactions of phenolic compounds based on high resolution mass spectrometry. *Atmos. Chem. Phys. Discuss.* **2010**, *10*, 4809–4822. [[CrossRef](#)]
19. Yu, L.; Smith, J.; Laskin, A.; Anastasio, C.; Laskin, J.; Zhang, Q. Chemical characterization of SOA formed from aqueous-phase reactions of phenols with the triplet excited state of carbonyl and hydroxyl radical. *Atmos. Chem. Phys. Discuss.* **2014**, *14*, 13801–13816. [[CrossRef](#)]
20. Yu, L.; Smith, J.; Laskin, A.; George, K.M.; Anastasio, C.; Laskin, J.; Dillner, A.M.; Zhang, Q. Molecular transformations of phenolic SOA during photochemical aging in the aqueous phase: Competition among oligomerization, functionalization, and fragmentation. *Atmos. Chem. Phys. Discuss.* **2016**, *16*, 4511–4527. [[CrossRef](#)]
21. Huang, D.D.; Zhang, Q.; Cheung, H.H.Y.; Yu, L.; Zhou, S.; Anastasio, C.; Smith, J.D.; Chan, C.K. Formation and Evolution of aqSOA from Aqueous-Phase Reactions of Phenolic Carbonyls: Comparison between Ammonium Sulfate and Ammonium Nitrate Solutions. *Environ. Sci. Technol.* **2018**, *52*, 9215–9224. [[CrossRef](#)]
22. Chen, H.; Ge, X.; Ye, Z. Aqueous-Phase Secondary Organic Aerosol Formation Via Reactions with Organic Triplet Excited States—a Short Review. *Curr. Pollut. Rep.* **2018**, *4*, 8–12. [[CrossRef](#)]
23. He, L.; Schaefer, T.; Otto, T.; Kroflič, A.; Herrmann, H. Kinetic and Theoretical Study of the Atmospheric Aqueous-Phase Reactions of OH Radicals with Methoxyphenolic Compounds. *J. Phys. Chem. A* **2019**, *123*, 7828–7838. [[CrossRef](#)] [[PubMed](#)]
24. Veres, P.; Roberts, J.M.; Burling, I.R.; Warneke, C.; De Gouw, J.; Yokelson, R.J. Measurements of gas-phase inorganic and organic acids from biomass fires by negative-ion proton-transfer chemical-ionization mass spectrometry. *J. Geophys. Res. Space Phys.* **2010**, *115*, 14033–14047. [[CrossRef](#)]
25. Desyaterik, Y.; Sun, Y.; Shen, X.; Lee, T.; Wang, X.; Wang, T.; Collett, J.L. Speciation of “brown” carbon in cloud water impacted by agricultural biomass burning in eastern China. *J. Geophys. Res. Atmos.* **2013**, *118*, 7389–7399. [[CrossRef](#)]
26. Kelly, J.M.; Doherty, R.M.; O'Connor, F.M.; Mann, G.W. The impact of biogenic, anthropogenic, and biomass burning volatile organic compound emissions on regional and seasonal variations in secondary organic aerosol. *Atmos. Chem. Phys. Discuss.* **2018**, *18*, 7393–7422. [[CrossRef](#)]
27. Pillar, E.A.; Zhou, R.; Guzman, M.I. Heterogeneous Oxidation of Catechol. *J. Phys. Chem. A* **2015**, *119*, 10349–10359. [[CrossRef](#)]
28. Pillar, E.A.; Guzman, M.I. Oxidation of Substituted Catechols at the Air–Water Interface: Production of Carboxylic Acids, Quinones, and Polyphenols. *Environ. Sci. Technol.* **2017**, *51*, 4951–4959. [[CrossRef](#)]
29. Tang, S.; Li, F.; Tsona, N.T.; Lu, C.; Wang, X.; Du, L. Aqueous-Phase Photooxidation of Vanillic Acid: A Potential Source of Humic-Like Substances (HULIS). *ACS Earth Space Chem.* **2020**, *4*, 862–872. [[CrossRef](#)]
30. Wang, J.; Wang, K.; Guo, Y.; Niu, J. Photochemical degradation of nebulivolol in different natural organic matter solutions under simulated sunlight irradiation: Kinetics, mechanism and degradation pathway. *Water Res.* **2020**, *173*, 115524. [[CrossRef](#)]
31. Anastasio, C.; Faust, B.C.; Rao, C.J. Aromatic Carbonyl Compounds as Aqueous-Phase Photochemical Sources of Hydrogen Peroxide in Acidic Sulfate Aerosols, Fogs, and Clouds. 1. Non-Phenolic Methoxybenzaldehydes and Methoxyacetophenones with Reductants (Phenols). *Environ. Sci. Technol.* **1997**, *31*, 218–232. [[CrossRef](#)]
32. Schauer, J.J.; Kleeman, M.J.; Cass, G.R.; Simoneit, B.R.T. Measurement of Emissions from Air Pollution Sources. 3. C1–C29 Organic Compounds from Fireplace Combustion of Wood. *Environ. Sci. Technol.* **2001**, *35*, 1716–1728. [[CrossRef](#)] [[PubMed](#)]
33. Schauer, J.J.; Cass, G.R. Source Apportionment of Wintertime Gas-Phase and Particle-Phase Air Pollutants Using Organic Compounds as Tracers. *Environ. Sci. Technol.* **2000**, *34*, 1821–1832. [[CrossRef](#)]
34. Nolte, C.G.; Schauer, J.J.; Cass, G.R.; Simoneit, B.R.T. Highly Polar Organic Compounds Present in Wood Smoke and in the Ambient Atmosphere. *Environ. Sci. Technol.* **2001**, *35*, 1912–1919. [[CrossRef](#)]
35. Arakaki, T.; Anastasio, C.; Kuroki, Y.; Nakajima, H.; Okada, K.; Kotani, Y.; Handa, D.; Azechi, S.; Kimura, T.; Tsuchi, A.; et al. A General Scavenging Rate Constant for Reaction of Hydroxyl Radical with Organic Carbon in Atmospheric Waters. *Environ. Sci. Technol.* **2013**, *47*, 8196–8203. [[CrossRef](#)]
36. Smith, J.D.; Kinney, H.; Anastasio, C. Phenolic carbonyls undergo rapid aqueous photodegradation to form low-volatility, light-absorbing products. *Atmos. Environ.* **2016**, *126*, 36–44. [[CrossRef](#)]
37. Tong, X.; Wang, S.; Wang, L. Kinetics and mechanism of syringic acid degradation initiated by hydroxyl radical and sulphate radical in the aqueous phase. *Chemosphere* **2020**, *256*, 126997. [[CrossRef](#)]
38. Smith, J.D.; Kinney, H.; Anastasio, C. Aqueous benzene-diols react with an organic triplet excited state and hydroxyl radical to form secondary organic aerosol. *Phys. Chem. Chem. Phys.* **2015**, *17*, 10227–10237. [[CrossRef](#)]

39. Liu, Y.; Lu, J.; Chen, Y.; Ye, Z.; Ge, X. Aqueous-Phase Production of Secondary Organic Aerosols from Oxidation of Dibenzothio-*phene* (DBT). *Atmosphere* **2020**, *11*, 151. [[CrossRef](#)]
40. Lee, A.K.Y.; Zhao, R.; Gao, S.S.; Abbatt, J.P.D. Aqueous-Phase OH Oxidation of Glyoxal: Application of a Novel Analytical Approach Employing Aerosol Mass Spectrometry and Complementary Off-Line Techniques. *J. Phys. Chem. A* **2011**, *115*, 10517–10526. [[CrossRef](#)]
41. Ye, Z.; Zhuang, Y.; Chen, Y.; Zhao, Z.; Ma, S.; Huang, H.; Chen, Y.; Ge, X. Aqueous-phase oxidation of three phenolic compounds by hydroxyl radical: Insight into secondary organic aerosol formation yields, mechanisms, products and optical properties. *Atmos. Environ.* **2020**, *223*, 117240. [[CrossRef](#)]
42. Onasch, T.B.; Trimborn, A.; Fortner, E.C.; Jayne, J.T.; Kok, G.L.; Williams, L.R.; Davidovits, P.; Worsnop, D.R. Soot Particle Aerosol Mass Spectrometer: Development, Validation, and Initial Application. *Aerosol Sci. Technol.* **2012**, *46*, 804–817. [[CrossRef](#)]
43. Cai, J.; Zeng, X.; Zhi, G.; Gligorovski, S.; Sheng, G.; Yu, Z.; Wang, X.; Peng, P. Molecular composition and photochemical evolution of water-soluble organic carbon (WSOC) extracted from field biomass burning aerosols using high-resolution mass spectrometry. *Atmos. Chem. Phys. Discuss.* **2020**, *20*, 6115–6128. [[CrossRef](#)]
44. Ge, X.; Li, L.; Chen, Y.; Chen, H.; Wu, D.; Wang, J.; Xie, X.; Ge, S.; Ye, Z.; Xu, J.; et al. Aerosol characteristics and sources in Yangzhou, China resolved by offline aerosol mass spectrometry and other techniques. *Environ. Pollut.* **2017**, *225*, 74–85. [[CrossRef](#)]
45. Chen, Y.; Li, N.; Li, X.; Tao, Y.; Luo, S.; Zhao, Z.; Ma, S.; Huang, H.; Chen, Y.; Ye, Z.; et al. Secondary organic aerosol formation from 3C\*-initiated oxidation of 4-ethylguaiaacol in atmospheric aqueous-phase. *Sci. Total Environ.* **2020**, *723*, 137953. [[CrossRef](#)] [[PubMed](#)]
46. Aiken, A.C.; Decarlo, P.F.; Kroll, J.H.; Worsnop, D.R.; Huffman, J.A.; Docherty, K.S.; Ulbrich, I.M.; Mohr, C.; Kimmel, J.R.; Sueper, D.; et al. O/C and OM/OC Ratios of Primary, Secondary, and Ambient Organic Aerosols with High-Resolution Time-of-Flight Aerosol Mass Spectrometry. *Environ. Sci. Technol.* **2008**, *42*, 4478–4485. [[CrossRef](#)]
47. Canagaratna, M.R.; Jimenez, J.L.; Kroll, J.H.; Chen, Q.; Kessler, S.H.; Massoli, P.; Ruiz, L.H.; Fortner, E.C.; Williams, L.R.; Wilson, K.R.; et al. Elemental ratio measurements of organic compounds using aerosol mass spectrometry: Characterization, improved calibration, and implications. *Atmos. Chem. Phys. Discuss.* **2015**, *15*, 253–272. [[CrossRef](#)]
48. Ye, Z.; Qu, Z.; Ma, S.; Luo, S.; Chen, Y.; Chen, H.; Chen, Y.; Zhao, Z.; Chen, M.; Ge, X. A comprehensive investigation of aqueous-phase photochemical oxidation of 4-ethylphenol. *Sci. Total Environ.* **2019**, *685*, 976–985. [[CrossRef](#)] [[PubMed](#)]
49. Zhang, Y.; Ren, H.; Sun, Y.; Cao, F.; Chang, Y.; Liu, S.; Lee, X.; Agrios, K.; Kawamura, K.; Liu, D.; et al. High Contribution of Nonfossil Sources to Submicrometer Organic Aerosols in Beijing, China. *Environ. Sci. Technol.* **2017**, *51*, 7842–7852. [[CrossRef](#)]
50. Kim, H.; Zhang, Q.; Heo, J. Influence of intense secondary aerosol formation and long-range transport on aerosol chemistry and properties in the Seoul Metropolitan Area during spring time: Results from KORUS-AQ. *Atmos. Chem. Phys. Discuss.* **2018**, *18*, 7149–7168. [[CrossRef](#)]
51. Zhao, R.; Aljawhary, D.; Lee, A.K.Y.; Abbatt, J.P.D. Rapid Aqueous-Phase Photooxidation of Dimers in the  $\alpha$ -Pinene Secondary Organic Aerosol. *Environ. Sci. Technol. Lett.* **2017**, *4*, 205–210. [[CrossRef](#)]
52. Gao, D.; Mulholland, J.A.; Russell, A.G.; Weber, R.J. Characterization of water-insoluble oxidative potential of PM<sub>2.5</sub> using the dithiothreitol assay. *Atmos. Environ.* **2020**, *224*, 117327. [[CrossRef](#)]
53. Saleh, R.; Hennigan, C.J.; Mcmeeking, G.R.; Chuang, W.K.; Robinson, E.S.; Coe, H.; Donahue, N.M.; Robinson, A.L. Absorptivity of brown carbon in fresh and photo-chemically aged biomass-burning emissions. *Atmos. Chem. Phys. Discuss.* **2013**, *13*, 7683–7693. [[CrossRef](#)]
54. Chen, Y.; Ge, X.; Chen, H.; Xie, X.; Chen, Y.; Wang, J.; Ye, Z.; Bao, M.; Zhang, Y.; Chen, M. Seasonal light absorption properties of water-soluble brown carbon in atmospheric fine particles in Nanjing, China. *Atmos. Environ.* **2018**, *187*, 230–240. [[CrossRef](#)]
55. Lin, P.; Laskin, J.; Nizkorodov, S.A.; Laskin, A. Revealing Brown Carbon Chromophores Produced in Reactions of Methylglyoxal with Ammonium Sulfate. *Environ. Sci. Technol.* **2015**, *49*, 14257–14266. [[CrossRef](#)]
56. Laskin, A.; Laskin, J.; Nizkorodov, S.A. Chemistry of Atmospheric Brown Carbon. *Chem. Rev.* **2015**, *115*, 4335–4382. [[CrossRef](#)] [[PubMed](#)]
57. Lambe, A.T.; Cappa, C.D.; Massoli, P.; Onasch, T.B.; Forestieri, S.D.; Martin, A.T.; Cummings, M.J.; Croasdale, D.R.; Brune, W.H.; Worsnop, D.R.; et al. Relationship between Oxidation Level and Optical Properties of Secondary Organic Aerosol. *Environ. Sci. Technol.* **2013**, *47*, 6349–6357. [[CrossRef](#)] [[PubMed](#)]
58. Vione, D.; Albinet, A.; Barsotti, F.; Mekic, M.; Jiang, B.; Minero, C.; Brigante, M.; Gligorovski, S. Formation of substances with humic-like fluorescence properties, upon photoinduced oligomerization of typical phenolic compounds emitted by biomass burning. *Atmos. Environ.* **2019**, *206*, 197–207. [[CrossRef](#)]
59. Xu, W.; Han, T.; Du, W.; Wang, Q.; Chen, C.; Zhao, J.; Zhang, Y.; Li, J.; Fu, P.; Wang, Z.; et al. Effects of Aqueous-Phase and Photochemical Processing on Secondary Organic Aerosol Formation and Evolution in Beijing, China. *Environ. Sci. Technol.* **2017**, *51*, 762–770. [[CrossRef](#)]
60. Liu, B.; Wu, S.-D.; Shen, L.-J.; Zhao, T.-X.; Wei, Y.; Tang, X.-L.; Long, C.-L.; Zhou, Y.; He, D.-W.; Lin, T.; et al. Spermatogenesis dysfunction induced by PM<sub>2.5</sub> from automobile exhaust via the ROS-mediated MAPK signaling pathway. *Ecotoxicol. Environ. Saf.* **2019**, *167*, 161–168. [[CrossRef](#)] [[PubMed](#)]
61. Wang, Y.; Zhang, M.; Li, Z.; Yue, J.; Xu, M.; Zhang, Y.; Yung, K.K.L.; Li, R. Fine particulate matter induces mitochondrial dysfunction and oxidative stress in human SH-SY5Y cells. *Chemosphere* **2019**, *218*, 577–588. [[CrossRef](#)] [[PubMed](#)]

62. Yu, S.; Liu, W.; Xu, Y.; Yi, K.; Zhou, M.; Tao, S.; Liu, W. Characteristics and oxidative potential of atmospheric PM<sub>2.5</sub> in Beijing: Source apportionment and seasonal variation. *Sci. Total Environ.* **2019**, *650*, 277–287. [[CrossRef](#)] [[PubMed](#)]
63. Chowdhury, P.H.; He, Q.; Male, T.L.; Brune, W.H.; Rudich, Y.; Pardo, M. Exposure of Lung Epithelial Cells to Photochemically Aged Secondary Organic Aerosol Shows Increased Toxic Effects. *Environ. Sci. Technol. Lett.* **2018**, *5*, 424–430. [[CrossRef](#)]
64. Zhou, J.; Zotter, P.; Bruns, E.A.; Stefenelli, G.; Bhattu, D.; Brown, S.; Bertrand, A.; Marchand, N.; Lamkaddam, H.; Slowik, J.G.; et al. Particle-bound reactive oxygen species (PB-ROS) emissions and formation pathways in residential wood smoke under different combustion and aging conditions. *Atmos. Chem. Phys. Discuss.* **2018**, *18*, 6985–7000. [[CrossRef](#)]